Resolving the upper-ocean warm layer improves the simulation of the Madden-Julian Oscillation

Wan-Ling Tseng[1,2], Ben-Jei Tsuang[3], Noel S. Keenlyside[4], Huang-Hsiung Hsu[1], & Chia-Ying Tu[1]

[1] *Research Center for Environmental Changes, Academia Sinica*

[2] *GEOMAR | Helmholtz-Zentrum für Ozeanforschung, Kiel, Germany.*

[3] *National Chung-Hsing University, Taichung, Taiwan.*

[4] Geophysical Institute and Bjerknes Centre, University of Bergen, Bergen, Norway.

Corresponding author: W.-L. Tseng, Research Center for Environmental Changes, Academia Sinica, Taipei, 115, Taiwan. (wtseng@gate.sinica.edu.tw)

TEL：886-2-2652-5174

FAX：886-2-2783-3584

Abstract

Here we show that coupling a high-resolution one-column ocean model to an atmospheric general circulation model (AGCM) dramatically improves simulation of the MJO to have realistic strength, period, and propagation speed. The mechanism for the simulated MJO involves both Frictional Wave-Convective Conditional Instability of the Second Kind (Frictional wave-CISK) and Air-Sea Convective Intraseasonal Interaction (ASCII). In particular, better resolving the

fine structure of upper ocean temperature, especially the warm layer, produces more vigorous atmosphere-ocean interaction and strengthens intraseasonal variations in both SST and atmospheric circulation. This helps organize and strengthen deep convection, inducing a stronger Kelvin-wave like perturbation and frictional near-surface convergence to the east. In addition, the warmer SST ahead of the MJO also acts to destabilize the boundary layer and enhance frictional convergence. These lead to a more realistic eastward-propagating MJO.

A suite of sensitivity experiments were performed to show the robustness of the mechanisms and to demonstrate: (1) that mean state differences are not the main contributors to the improved simulation of our coupled model; (2) the role of SST variability in enhancing frictional convergence and intraseasonal variations in precipitation, and (3) that the simulation is significantly degraded when the first ocean model layer is thicker than 10m. Our coupled model results are consistent with observations and demonstrate a simple but effective means to significantly improve MJO simulation and potentially also forecasts.

Key word: MJO, Coupling, warm layer, one column ocean model

1. Introduction

The Madden-Julian Oscillation (MJO) is the dominant pattern of atmospheric intraseasonal variability in the tropics. MJO events are characterized by large-scale tropical circulation anomalies that develop over the Indian Ocean and propagate eastward into the western Pacific with a timescale of 2-3 weeks (Madden and Julian 1972; Hendon and Salby 1994; Zhang and Mu 2005). Many theories exist for the MJO, but none are completely satisfactory. The equatorial wave solution to deep tropical diabatic heating describes the MJO structure well, but fails to explain its period of 30-60 days and eastward propagation speed of approximately 5 m/s over the Indo-Pacific warm pool[1] (Madden and Julian 1972; Zhang 2005). On these timescales, low-level moisture convergence, warm sea surface temperature (SST), and shallow upper ocean mixed-layer depth precede the eastward propagation of organized deep convection by around ten days (Hendon and Salby 1994; Woolnough et al. 2000); opposite conditions follow by around 10 days. While the oceanic changes are well understood (Shinoda and Hendon 1998; Bernie et al. 2005), the relative importance of the low-level convergence and ocean-atmosphere interaction are debated (Zhang et al. 2006; Marshall et al. 2008).

There are numerous MJO theories. Some of them disagree on the cause of the low-level convergence. For example, in Frictional Wave-Convective Conditional Instability of the Second Kind (Frictional wave-CISK), equatorial waves propagate eastward through the interaction with the frictional boundary layer (Wang and Rui 1990; Hendon and Salby 1994; Maloney and Hartmann 1998; Hsu et al. 2004; Kang et al. 2013). While in Air Sea Convective Intraseasonal Interaction (ASCII) (Flatau et al. 1997; Waliser et al. 1999), the SST drives the low-level convergence and eastward propagation, but the exact mechanism remains unclear. Other theories emphasize different aspects. In the wind-evaporation feedback or wind induced surface heat exchange (WISHE) theory (Emanuel 1987; Neelin et al. 1987), the destabilization of the convectively coupled Kelvin wave is driven by anomalous latent heat flux at the surface induced by anomalous wind speed. This theory cannot explain the eastward propagation in the Indian Ocean and the western Pacific where the observed background flow is

[1] Typically defined as the region of water warmer than 29°C in the Indo-Pacific region.

westerly. Although the increased moisture preceding the MJO does not result from locally enhanced evaporation, the feedback of moisture and heat flux on the MJO is likely important (Maloney and Sobel 2004; Maloney 2009; Kiranmayi and Maloney 2011; Andersen and Kuang 2012). Multi-scale interaction during the MJO is also observed (Nakazawa 1988; Hendon and Liebmann 1994; Chen et al. 1996; Yanai et al. 2000; Zhang 2005). The eastward moving convective center or active phase of the MJO can be viewed as a large-scale ensemble of myriad higher-frequency, small-scale convective systems moving in all directions. Large-scale dynamics may organize the mesoscale convective systems, which in turn can couple shallow and deep heating modes, leading to eastward propagating MJO like disturbances (Ajayamohan et al. 2013).

It remains a challenge to simulate the MJO. Only a limited number of atmospheric models were shown to simulate the MJO reasonably well (Lin et al. 2006; Kim et al. 2009; Jiang et al. 2014). Model disagreement has been linked to differences in the representation of atmospheric processes, such as convection and boundary layer processes (Liu et al. 2005; Zhang and Mu 2005; Zhu et al. 2009; Deng and Wu 2010; Zhou et al. 2012). The simulation of the MJO is also sensitive to the background mean state including westerly winds and precipitation that are often poorly simulated by coupled models (Inness and Slingo 2003; Watterson and Syktus 2007; Kim et al. 2011).

There is some consensus that coupling with an ocean model generally improves an atmospheric model's simulation of the MJO. However, most current coupled models still poorly simulate intraseasonal atmospheric variability (Kim et al. 2011; Hung et al. 2013) and the role of coupling remains debated. In particular, while in some models resolving ocean-atmosphere interaction benefits MJO simulation (Waliser et al. 1999; Inness and Slingo 2003; Marshall et al. 2008; Klingaman et al. 2011; Subramanian et al. 2011; Crueger et al. 2013), in others it has little influence or even degrades model performance (Hendon 2000; Sperber et al. 2005; Hung et al. 2013).

In terms of the oceanic aspect, coupling to an ocean general circulation model (OGCM) (Bernie et al. 2008), a simple slab ocean model (Marshall et al. 2008) or a more complex 1D ocean mixed layer model (Bernie et al. 2005) have all been shown to improve the simulation of the MJO. Bernie et al. (2008) showed that resolving the diurnal cycle in the upper ocean improves coupled ocean-atmosphere feedbacks, the basic state, and the timing of the seasonal cycle of SST and the trade winds in the tropical Pacific, and leads to a better simulation of the MJO. These effects represent a non-linear rectification of the diurnal cycle onto intraseasonal variability and the mean state. Woolnough et al. (2007) compared a fully coupled atmosphere-ocean model and an atmosphere-1D ocean mixed layer model for MJO prediction skill. Their experiment with the mixed layer model showed improvement in skill over the full dynamical ocean model that arises from an enhanced sensitivity of the SST to the surface flux. Other works have examined the sensitivity to slab thickness in coupled AGCM – slab ocean models (Watterson 2002; Maloney and Sobel 2004; Klingaman et al. 2011). In general, shallower slabs resolve upper ocean temperature variance better and further improve the MJO simulation. However, most climate models do not resolve upper ocean processes sufficiently to simulate realistically intraseasonal SST variations in the Indo-Pacific warm pool region. Thus, the role played by SST variations on these timescales in the MJO remains to be fully explored.

To better simulate the upper ocean temperature variability in the Indo-Pacific warm pool it is necessary to include the processes that determine the warm layer and cool skin. The warm layer (Fairall et al. 1996) resides in the upper few meters of the ocean, where most of the solar radiation is absorbed. It onsets after sunrise, exists until sunset, and is a maximum in the early afternoon. The warm-layer contributes to the diurnal cycle in SST. The cool-skin phenomenon occurs because energy transport is limited to molecular diffusivity in the upper few tenths of a millimeter to a few millimeters, depending on wind speed (Fairall et al. 1996; Tu and Tsuang 2005). This phenomenon causes the SST to be typically a few-tenths of a degree Celsius cooler than the temperatures below (Saunders 1967; Paulson and Simpson 1981; Wu 1985; Fairall et al. 1996). The cool skin does not contribute directly to SST variability, but is important for computation of surface fluxes.

In summary, our theoretical understanding and ability to simulate the MJO are limited, and while it is generally accepted that ocean-atmosphere interaction improves the simulation of the MJO, whether it is an essential element of the MJO is unclear. The main objective of this study is to improve understanding of the role of ocean-atmosphere interaction for the MJO. In particular, we aim to address two open issues: First, what is the role of temperature variations in the upper few meters of the ocean? We also consider the influence of the cool-skin, but find very limited impact on the MJO; thus it is not discussed further. Second, what is the role of the SST in driving low-level convergence? Is it a local or remote influence? For this purpose, we couple a high-vertical-resolution 1D ocean mixed layer model to an atmospheric general circulation model (AGCM) with high coupling frequency. The model configuration allows proper simulation of upper-ocean temperature variations, while maintaining a realistic model mean state. The coupling substantially improves simulation of the MJO to have realistic strength, period, and propagation speed. In our opinion, the model performance surpasses that of most previous studies; it is also listed among the eight best models in simulating the MJO and four best in simulating convectively coupled wave spectra in a recent intercomparison of 27 models (Jiang et al. 2014). A suite of carefully designed experiments are performed to identify the contribution of mixed-layer processes, the key regions of ocean-atmosphere interaction, mean state differences, and intraseasonal SST variations in our improved MJO simulation. The model and methods are described in the next section. Section 3 presents the results and is followed by a summary and discussion.

2. Data, methodology and model

We analyse Global Precipitation Climatology Project (GPCP) data, outgoing longwave radiation (OLR) and daily SST (OISST; Reynolds and Smith (1995)) data from the National Oceanic and Atmosphere Administration (NOAA) and parameters from ERA-interim reanalysis (Dee et al. 2011). We use the CLIVAR MJO Working Group diagnostics package (CLIVAR 2009), and a 20-100 day filter to isolate intraseasonal variability. MJO phase composites are computed using the MJO index defined by the leading pair of principal components from an Empirical Orthogonal Function analysis of intraseasonal OLR, and 850 hPa and 200 hPa zonal wind (Wheeler and Hendon 2004).

The model used in this study is ECHAM5.4 (Roeckner 2003) coupled with the Snow-Ice-Thermocline (SIT) one column ocean model (Tu and Tsuang 2005; Tsuang et al. 2009). ECHAM5 is the fifth generation of the ECHAM atmospheric general circulation model, developed at the Max Planck Institute for Meteorology (MPI). It is a spectral model employing state-of-the-art physics. The horizontal resolution used here is T63 (~1.8°) with 31 vertical layers and a model top at 10hPa (~30km). The default cumulus convective scheme, Nordeng (Nordeng 1994), is used in this study. Nordeng is an improved version of the Tiedtke mass flux convection scheme (Tiedtke 1989). Nordeng extends on this scheme to have organized entrainment and detrainment in penetrative convection related to buoyancy.

SIT simulates the SST and upper ocean temperature variations, including the cool skin and warm layer (diurnally occurring) of the upper ocean, and turbulent kinetic energy (TKE;Gaspar et al. (1990)) of a water column. Further details of the SIT model are described in the appendix. In the finest resolution experiments SIT has 42 vertical layers, with 12 in the upper 10 m. The resolution in the upper 10 m is very fine in order to capture the upper ocean warm layer, and there is a layer at 0.05 mm for reproducing the cool skin of the ocean surface. Note that it is not conventional to couple such a high vertical resolution TKE ocean model to an AGCM. To account for neglected horizontal processes, the ocean is weakly nudged (with a 30-day time scale) to the observed climatological ocean temperature below 10 m depth; there is no nudging within the upper 10-m depth. SIT and ECHAM exchange SST and fluxes at every time step (12 minutes) in the tropics (30°S-30°N), elsewhere climatological SST drives the AGCM.

A series of 25-year numerical experiments were performed to evaluate the impact of atmosphere-ocean coupling on the MJO simulation. They include a control coupled simulation (C-CTL) and standalone AGCM simulations forced by observed and simulated climatological monthly SST (A-CTL and A-clim, respectively) and daily SST

(A-OISST and A-day, respectively). Note that in the coupled simulations, model SST was relaxed to observed climatological monthly SST (see appendix). Two extra coupled experiments with coarser vertical resolutions (16.8 meters (C-17m) and 59.3 meters (C-59m); see appendix) in SIT and three regional coupled experiments (the Indian Ocean (C-IO), the western Pacific (C-PO) and the Indian-western Pacific Oceans (C-IPO)) were also conducted. All experiments are summarized in the Table 1.

3. Simulation results

3.1. The improvement of MJO simulation through ocean-atmosphere coupling

To assess the impact of ocean-atmosphere interaction on the MJO, we compare simulations of the coupled model (C-CTL) with the uncoupled AGCM (A-CTL) forced by climatological monthly SST. We focus on boreal winter (November-April) when the MJO is most prominent, but results are similar in other seasons (not shown). As shown in zonal wavenumber-frequency spectra of 850-hPa zonal wind (Fig. 1a-c), the coupled model simulates realistically the 30-80-day eastward-propagating zonal-wavenumber one signal. The uncoupled AGCM produces both eastward and westward propagating wavenumber 1-3 signals with periods longer than 80 days, indicative of the stationary behavior of the uncoupled simulation. The coupled model reproduces the realistic eastward propagation, although slightly slower than observed, in precipitation and surface winds, in contrast to the stationary intraseasonal fluctuation in the uncoupled simulation (e.g., Hovmöller diagrams shown in Fig. 1d-f). This statistical analysis clearly shows the improvements of the MJO simulation in the coupled model relative to the uncoupled simulation. Thus, active ocean-atmosphere interaction may be an important factor responsible for the coupled model’s realistic MJO simulation

(Watterson 2002; Watterson and Syktus 2007; Woolnough et al. 2007; Subramanian et al. 2011; Crueger et al. 2013). In contrast to other state-of-the-art climate models (Kim et al. 2009; Hung et al. 2013), ECHAM-SIT exhibits excellent MJO simulation skill both in the periodicity and eastward propagation, and is among the few top models participating in a Joint WGNE MJO Task Force / GEWEX GASS Project on the Vertical Structure and Diabatic Processes of the MJO - Part I. Climate Simulations (Jiang et al. 2014).

3.2.Mechanism investigation

In this section two possible mechanisms for the improved MJO simulation resulting from coupling are investigated, and their relevance to observations is discussed.

a) Instability

We analyze vertical atmospheric profiles and local ocean-atmosphere interaction in different MJO phases over the Maritime Continent region; these results are representative for the entire Indo-Pacific warm pool sector. Figure 2 shows MJO phase composites analysis for the vertical profile of moisture divergence and the equivalent potential temperature (θ_e) over the 10°S-0°N and 120-150°E region. In both observations and the coupled simulation, near-surface moisture convergence and a less stable lower troposphere (during phase 1-3) lead the deep convection (in phase 4) (Fig. 2a, b; upper panels). As the MJO is an eastward propagating phenomenon, the shallow convective phases occur to the east of deep convective phases and hence, the horizontal (phase) axis can be equivalently considered as the zonal direction (Kim et al. 2009).

Thus the moisture convergence exhibits a westward titling structure that is consistent with low-level convergence preconditioning deep convection and the eastward propagation. The uncoupled AGCM fails to simulate both enhanced low-level moisture convergence and less stable lower troposphere during the development phase (Fig. 2c).

The simulated intraseasonal SST variations largely agree with observations in terms of amplitude and phase, although the model warm phase leads the observed by about a phase. By contrast, there is no intraseasonal SST variation in the uncoupled model (Fig 2; bottom) because of prescribed climatological monthly SST. The observed SST varies by a few tenths of a degree over an MJO life cycle, with positive 2m temperature (T2m), negative (anomalously downward) latent heat flux, negative sensible heat flux (not shown), and positive (anomalously downward) short wave flux (not shown) anomalies leading warmer SST, and vice versa for cooler SST (Fig. 2a). Both latent and sensible heat flux variations are dominated by anomalous wind speed, but sensible heat flux variations are much weaker than those of latent heat flux. While the latent heat flux variations in the coupled and uncoupled simulations have similar phase relation to observations, major differences are found in the simulation of T2m. In the MJO development phase, the T2m anomaly is positive in the coupled simulation, but it is negative in the uncoupled simulation. This might be because the SST does not vary in the uncoupled simulation and the negative sensible heat fluxes cool the atmosphere (not shown). In the coupled model the T2m temperature appears more synchronized with the SST in comparison to ERA-interim reanalysis, but there is large uncertainty between reanalysis data (e.g., comparing the ERA-Interim and NCEP reanalysis in bottom panel of Fig 2a). The NCEP reanalysis also shows a near synchronization between T2m and SST. In observations the warmer SST appears almost concurrently with near-surface convergence, and both lead the deep convection (Fig. 2a). This well-known phase relationship is reasonably simulated by the coupled model, but cannot be simulated by the uncoupled model with prescribed SST (Fig. 2; bottom panel). In observations and the coupled model the warmer SST contribute to destabilize the lower troposphere during the MJO's development, consistent with the ASCII mechanism. However, in the uncoupled simulation, the fixed climatological SST stabilizes and weakens low-level convergence. This stabilization effect is unfavorable for triggering the low-level convergence. The convergence may also in part be driven by large-scale influences, as discussed further below.

To further understand the moisture sources (Fig. 2), the moisture flux divergence on the intraseasonal time scale is decomposed as follows:

$$
\begin{aligned}
&(\nabla \cdot \mathrm{q}\vec{\mathrm{U}})' \\
&= [q]\frac{\partial u'}{\partial x} + [q]\frac{\partial v'}{\partial y} + [u]\frac{\partial q'}{\partial x} + [v]\frac{\partial q'}{\partial y} + q'\frac{\partial [u]}{\partial x} + q'\frac{\partial [v]}{\partial y} + u'\frac{\partial [q]}{\partial x} + v'\frac{\partial [q]}{\partial y} \\
&+ q'\frac{\partial u'}{\partial x} + q'\frac{\partial v'}{\partial y} + u'\frac{\partial q'}{\partial x} + v'\frac{\partial q'}{\partial y}
\end{aligned}
$$

where, q is specific humidity, and $\vec{u}$ is vector wind. Brackets are climatological means, and primes are intraseasonal anomalies. Results are presented in Fig. 3. In observation and coupled model the anomalous low-level moisture convergence is mainly determined by anomalous wind convergence (i.e., the first two right-hand terms), while other terms are of secondary importance. The moisture convergence in the uncoupled simulation remains small in all phases compared to the observation and the coupled simulation. The meridional component ($[q]\frac{\partial v'}{\partial y}$) that is a dominant term in moisture flux convergence is missing in the uncoupled simulation. The anomalous wind convergence drives the moistening of atmospheric boundary layer and preconditions the atmosphere for deep convection leading to the active MJO phase and eastward propagation. The coupled model successfully simulated this important process.

b) Precipitation and Kelvin wave

Stronger convection will help trigger stronger convectively coupled equatorial waves. Thus, another possible reason for the improved coupled model simulation is the increase in precipitation variability of up to 180% over parts of the Indian Ocean and the Maritime Continent compared to the uncoupled model (Fig. 4). This appears to lead to more organized convection and stronger Kelvin-wave like signals with enhanced low-level convergence to the east of the convection. This is evident in composites for phase 4 when deep convection is the strongest over the Maritime Continent (Fig. 5); similar results are found for phase 3. During these phases, SLP pattern in the observation and the coupled model resembles the classical Gill-type (Gill 1980) response to tropical heating, while the pattern in the uncoupled model is not as well organized (Fig. 5a, c and e). Although both models simulate Kelvin-wave like SLP structure leading the convection, only the coupled model is able to reproduce the low-level wind convergence strongly confined to the equator as in observations. In the uncoupled model low-level convergence occurs only in limited regions with no clear relationship with the deep convection. The convergence in both the observation and the coupled simulation does not coincide with the warmest water (Fig. 5b, d) and therefore is not completely consistent with the Lindzen-Nigam model (Lindzen and Nigam 1987). The Kelvin-wave like structure with the meridional low level convergence is consistent with the Frictional Wave-CISK mechanism that acts as a major mechanism in both observation and our coupled model. The improved MJO simulation is shown to be due to active ocean-atmosphere interaction, and the mechanism identified appears to have elements of Frictional wave-CISK and ASCII.

3.3. Sensitivity experiments

In this section we will address the importance of vertical resolution and investigate the regions where coupling is most essential. Furthermore, we will consider whether the improvements arise indirectly through accounting for intraseasonal SST variations or through changes in the background state, rather than active ocean-atmosphere interaction.

a) Ocean vertical resolution

Two additional experiments are performed to further assess the SST's role in determining the eastward propagation speed and period of the MJO. In the coupled model experiment (C-CTL) described above the vertical resolution is 1m within the upper 10m, while in the two new experiments the top of the ocean layer is increased to 16.8m (C-17m), and 59.3m (C-59m), respectively. In the C-CTL simulation the upper ocean temperature variations are mostly confined to the upper 10m of the ocean and are the largest in the upper few meters (Fig. 6a). The amplitude of the temperature variations over the MJO cycle decreases by about 20% in the C-17m (Fig. 6b), and by about 40% in the C-59m (Fig. 6c). Furthermore, the coarser the resolution the slower the temperature response to the surface heating changes, as thicker surface layers heat more slowly. This causes a longer intraseasonal periodicity and slower eastward propagation of the MJO (Fig 6d-f). These results suggest temperature variations in the upper few meters of the ocean contribute to setting the MJO periodicity in this model.

b) Regional coupling experiments

Here we consider three experiments that examine the importance of the ocean-atmosphere interaction over different regions of the main MJO activity area with coupling (1) over the Indian Ocean (C-IO; 30°N-30°S, 50°E-100°E), (2) over the western Pacific (C-PO; 30°N-30°S, 110°E-180°E), and (3) over both regions (C-IPO; 30°N-30°S, 40°E-180°E); elsewhere observed climatological SST is prescribed. The C-IPO run exhibits the best MJO simulation (Fig. 7c and 7f) in terms of the zonal wave number-frequency spectrum and eastward propagation characteristics. The simulation of the MJO is degraded in the C-IO and C-PO runs (Fig. 7a-b, d-e) when coupling was performed only in one oceanic region. The result tends to relax toward that of the uncoupled simulation (i.e., the A-CTL), e.g., longer periodicity and weaker eastward propagation tendency. Key discrepancies are found in the phase 4 of MJO life cycle in the different experiments (Fig. 8). The C-IPO correctly reproduces the SSTA-convergence relationship in the observation and the C-CTL simulation. In the C-IO and C-PO experiments, the SSTA-convergence relationship is correctly simulated in the oceanic region where coupling is considered. By contrast, in other regions the near-surface convergence is much weaker than the observed and that in the C-CTL. The C-PO simulates stronger eastward-propagation tendency and near-surface convergence in the western Pacific than the C-IO. The warm SST anomalies over the western Pacific act to destabilize the boundary layer, and help drive the near surface convergence and eastward propagation of the MJO. In addition, the intraseasonal precipitation variance in the tropical eastern Indian Ocean and the Maritime Continent is also enhanced due to the coupling. Fig. 9 shows the same intraseasonal precipitation variance ratio for the regional coupling experiments, as in Fig. 4. The precipitation variance in the southeastern Indian Ocean and the western Maritime Continent in the C-IPO is similar to the C-CTL experiments and is the largest, followed by the C-PO and C-IO. A comparison between Fig. 8 and Fig. 9 indicates that larger intraseasonal precipitation variance ratio corresponds to stronger near-surface convergence along the equator in the western Pacific. Results presented above confirm again that the coupling enhances both ASCII and Frictional wave-CISK mechanisms and therefore is an important process for simulating realistic MJO.

c) Daily SST variations and mean state discussion

In this section we consider three experiments designed to assess the importance of time varying SST versus active ocean-atmosphere coupling and further discuss the mean state effect. These experiments consist of uncoupled experiments forced by observed daily SST (A-OISST), simulated daily SST from the C-CTL (A-day) and simulated climatological monthly SST from the C-CTL (A-clim). The impact on the MJO is assessed in terms of zonal-wavenumber spectrum and eastward propagation of intraseasonal precipitation and 10m zonal wind. A comparison between the A-OISST (with daily SST, Fig. 10a and d) and the A-CTL (with climatological monthly mean SST, Fig. 1c and 1f) indicates that the simulation including the intraseasonally-varying SST signal does not help much in improving the simulation of periodicity and eastward propagation. By contrast, forcing the model with simulated daily SST (Fig. 10b and e) does simulate stronger eastward propagation tendency, although the frequency is still lower than the observed. When the simulated climatological monthly mean SST is used as a forcing, the simulation results deteriorate (Fig. 10c and 10f). This comparison between different SST simulations suggests higher-frequency SST variations help improve the eastward propagation but have little effect on improving the periodicity simulation. The contrast between the C-CTL (coupled) and the A-day (uncoupled) further suggests that the coupling tends to synchronize and enhance the internal oceanic and atmospheric variability on intraseasonal timescales.

One interesting point is the improvement of the A-day simulation over the A-OISST simulation. Fig 11 shows the SST-convergence relationship in both simulations in phase 4. Near-surface convergence and SSTA in the A-OISST simulation are weaker than those in the A-day simulation. In the A-OISST simulation, the near-surface convergence in the western Pacific is located off the equator and the model does not realistically simulate the equatorial Kelvin wave as observed (not shown). It is likely that the Frictional wave-CISK mechanism does not work properly when the observed daily SST is prescribed. By contrast, the observed convergence-SSTA relationship is reasonably simulated in the A-day simulation. The much larger intraseasonal variance of precipitation (Fig. 12) in A-day simulations than in the A-OISST simulation also induce more active equatorial waves, as in those simulations shown in preceding sections. Although the OISST is the observation and represents the true world, it does not seem to synchronize nicely with the simulated circulation in the model, perhaps because our model simulates slower MJO eastward propagation than observed (Fig. 1). By contrast, the simulated SSTA seems to synchronize much closely with the circulation in the model, probably due to the imprinted influence of the model circulation through coupling. This result is consistent with Woolnough et al. (2000).

The simulation of the MJO is recognized to be sensitive to the mean state (Watterson and Syktus 2007; Kim et al. 2011). Thus, one would be interested in whether better MJO simulation is associated with an improved simulation of mean flow. Climatological mean 10-m zonal wind, precipitation, and SST in the observation and in the C-CTL, A-CTL, and A-clim simulations are presented in Fig. 13. In terms of MJO performance, the C-CTL simulation is the best, followed by the A-clim and A-CTL simulations. A statistical significance test was conducted between the fields shown in Fig. 13. No significant differences were found between C-CTL and A-clim simulations in terms of wind and precipitation fields over the tropics (not shown). This is consistent with the A-clim simulation being forced by the climatological monthly SST from the C-CTL simulation. The improvement of MJO simulation in the C-CTL experiment over the A-clim experiment is evidently due to the coupling. A comparison between the A-clim and A-CTL experiments yields another interesting point. While the A-CTL experiment simulates a better spatial distribution of precipitation compared to the A-clim experiment, the precipitation in the eastern Indian Ocean and the western Maritime Continent is significantly under simulated. By contrast, the A-clim simulates much larger mean precipitation and also stronger variance (not shown), although the westerly in the eastern Indian Ocean and the Maritime Continent is weaker. In summary, the comparison of A-clim to A-CTL shows the mean state has an effect on the MJO simulation and may explain some of the discrepancies in our simulation to observations. But the comparison of C-CTL to A-clim indicates that the ocean-atmosphere coupling is a more influential process than the mean states for improving MJO simulation in this study; this might be because our model already simulates a mean state favorable to the simulation of the MJO. Independently performed experiments with CNRM show a similar importance of air-sea interaction (Jiang et al. 2014).

4. Summary

This study has shown that coupling SIT, a 1-D TKE ocean mixed layer model, to the ECHAM5 significantly improves the MJO simulation over the stand-alone ECHAM5 and produces a much better result than most of the current climate models (Kim et al. 2009; Hung et al. 2013; Jiang et al. 2014). The ECHAM5-SIT is a simple and efficient way to simulate the major MJO characteristics (e.g., periodicity, eastward propagating speed, vertical structure, etc.). Our results suggests the MJO can be more realistically simulated by increasing the vertical resolution of the one-column ocean model to better resolve the upper-ocean warm layer. The improvement and the effect of the warm layer have not been demonstrated so clearly in previous studies. This study supports the previous findings that coupling may improve the MJO simulation, although the ocean may simply play a passive role in response to atmospheric forcing, by clearly demonstrating the potential of coupling processes for a significant improvement in MJO simulation.

The performance of the ten 25-year simulations conducted in this study is summarized in terms of four common metrics in Fig. 14. Fig. 14a presents the propagation speed of the MJO (based on 10-meter zonal wind) versus power ratio of eastward- and westward-propagating 30-80-day signal (E/W ratio, derived from the zonal wavenumber-period spectrum; Kim et al. (2009)). Fig. 14b presents the propagation speed of MJO-related precipitation anomaly versus the variance explained by RMM1 and RMM2 (e.g., the sum of the EOF1 and EOF2 variance based on Wheeler and Hendon 2004). Considering all four metrics, the C-CTL and A-CTL simulate yield the best and worst performance, respectively. MJO simulation skill decreases when air-sea interaction is degraded, as demonstrated in the regional coupling simulations (purple; C-IO, C-PO and C-IPO), as well as in simulations of coarser vertical ocean resolution (blue; C-17m and C-59m). Uncoupled simulations generally show lower skill than the coupled simulations. Characteristics of SST prescribed in the uncoupled simulation affect the simulation skill. Using daily or simulated SST is able to enhance the E/W ratio and eastward propagation, but both are still under simulated compared to the coupled simulation and observations. Comparing the A-clim and A-CTL simulations (i.e., with coupled and observed climatological monthly SST, respectively) shows that the mean state improves the MJO simulation to some extent but coupling is needed for a realistic simulation. This can be seen more clearly by comparing Fig. 1 and 10. Prescribing observed and simulated daily SST also improves MJO simulation, but the frequency is unrealistically low.

This study suggests that SST variations may improve the simulation of intraseasonal atmospheric variability over the Indo-Pacific warm pool region. We identify two possible reasons for the coupled model's better MJO simulation. First, the coupled simulation reproduces the observed warmer SST leading the convectively active MJO phase that contributes to destabilize the boundary layer. Second, coupling enhances precipitation variability on intraseasonal timescales, which results in stronger and more organized diabatic heating and tropical waves. Together these two factors enhance the low-level atmospheric convergence ahead of the MJO. The sensitivity studies supported the importance of these two factors in the simulation of the MJO.

Thus, the mechanism suggested by our results (Fig. 15) has elements of the Frictional wave-CISK and ASCII mechanisms. It is reminiscent of the "enhanced moisture convergence-evaporation feedback" (EMCEF) mechanism of Marshall et al. (2008) with the only difference being the sign of latent heat flux anomalies ahead of and behind the MJO convection. Our mechanism can be summarized as follows: To the east of organized deep convection there is increased incident short wave radiation due to clear sky conditions, and reduced latent heat flux (evaporation) from weaker wind speed. These drive the warming of the upper ocean. The organized deep convection induces a Kelvin-wave like perturbation with lower SLP to the east at the equator. The latter enhances the low-level atmospheric convergence through frictional effects and leads to enhanced low-level moisture, preconditioning deep convection and eastward propagation of deep convection; while the warmer ocean enhances frictional convergence. To the west, stronger winds enhance evaporation and latent heat flux loss, and cool the ocean; while under the deep convection short wave radiation is reduced and also cools the ocean. Weaker winds ahead of the deep convection and stronger winds following drive shallow and deep upper ocean mixed layers, respectively. In this way ocean-atmosphere interaction appears a key element of the MJO, helping to drive eastward propagation of intraseasonal atmospheric variability and set the dominant timescale.

We examined two specific issues here. First, what is the role of temperature variations in the upper few meters of the ocean? Our results are consistent with the previous studies (Watterson 2002; Woolnough et al. 2007; Klingaman et al. 2011) that coupling improves MJO simulation. This study further demonstrates the significant improvement achieved through the two mechanisms mentioned above by a passive but essential ocean role, especially the warm layer temperature variability. In addition to confirming that shallower mixed layer could accelerate the MJO eastward propagation speed (Watterson 2002), our simulations also provide the precise evidence that the fine ocean vertical resolution is necessary to well reproduce warm layer. Second, what is the role of the SST in driving low-level convergence? Is it local or remote influence? Locally, warmer SST destabilizes the lower troposphere during the MJO development phase. In addition, stronger Kelvin wave signal could be induced by remote influence of the enhanced deep convection due to coupling. This is an important concept to further understand the detail of the ocean-atmosphere coupling process.

It is interesting that, while the mean state changes do help to certain extent, it is not the most influential factor in simulation improvement, as we demonstrated by performing an additional uncoupled experiment with prescribed SST from the fully coupled model (Fig. 1 and 10). This simulation reproduced the mean state of the ECHAM5-SIT coupled model, but the MJO simulation was less realistic. Our results do not necessarily contradict previous findings showing the sensitivity of MJO simulation to the background mean state (e.g., Inness et al. 2003; Watterson and Syktus 2007; Kim et al. 2011a). Instead, it simply indicates that coupling has a stronger effect in improving MJO simulation in our model; this might be because our model already simulates a mean state favorable to the simulation of the MJO. A similar finding has been recently reported (Jiang et al. 2014).

Our results suggest that accurate simulation of the MJO can be achieved by a fine oceanic vertical resolution that can capture temperature variations in the upper few meters of the ocean. Nevertheless, many other atmospheric factors (e.g., realistic representation of the climatology and convective parameterization) are known to influence the MJO, which is essentially an atmospheric mode of variability (Zhang 2005; Ajayamohan et al. 2013). Coupling may only improve MJO simulation in AGCMs with reasonable atmospheric dynamics and parameterization schemes. Nevertheless, this study provides a great promise for future prediction of MJO variability and its impacts.

Acknowledgments. The Deutsches Klimarechenzentrum, the Norddeutscher Verbund für Hoch- und Höchstleistungsrechnen and Taiwan/NCHC provided computing resources. The Deutsches Forschungsgemeinschaft under the Emmy Noether-Programm (KE 1471/2-1), the German BMBF NORDATLANTIK project, DFG-NSC international cooperation grant, and EU SUMO (266722) and, STEPS (PCIG10-GA-2011-304243), and PREFACE (603521) projects provided financial support. The National Science Council, Taiwan, also supported the work (Grant NSC-100-2119-M-001-029-MY5; NSC 99-2111-M-005-001-MY3; NSC 102-2627-B-005-006-). We are grateful to the National Center for High-performance Computing for computer time and facilities. The Max Planck Institute for Meteorology provided the ECHAM5.

References

Adler RF, Huffman GJ, Chang A, Ferraro R, Xie P-P, Janowiak J, Rudolf B, Schneider U, Curtis S, Bolvin D (2003) The version-2 global precipitation climatology project (GPCP) monthly precipitation analysis (1979-present). Journal of Hydrometeorology 4 (6):1147-1167

Ajayamohan R, Khouider B, Majda AJ (2013) Realistic initiation and dynamics of the Madden-Julian Oscillation in a coarse resolution aquaplanet GCM. Geophysical research letters 40 (23):6252-6257

Andersen JA, Kuang Z (2012) Moist static energy budget of MJO-like disturbances in the atmosphere of a zonally symmetric aquaplanet. Journal of Climate 25 (8):2782-2804

Bernie D, Guilyardi E, Madec G, Slingo J, Woolnough S, Cole J (2008) Impact of resolving the diurnal cycle in an ocean–atmosphere GCM. Part 2: A diurnally coupled CGCM. Climate Dynamics 31 (7-8):909-925

Bernie D, Woolnough S, Slingo J, Guilyardi E (2005) Modeling diurnal and intraseasonal variability of the ocean mixed layer. Journal of climate 18 (8):1190-1202

Chen SS, Houze Jr RA, Mapes BE (1996) Multiscale variability of deep convection in realation to large-scale circulation in TOGA COARE. Journal of the Atmospheric Sciences 53 (10):1380-1409

CLIVAR MJOWG (2009) MJO Simulation Diagnostics. Journal of Climate 22 (11):3006-3030

Crueger T, Stevens B, Brokopf R (2013) The Madden-Julian Oscillation in ECHAM6 and the introduction of an objective MJO metric. Journal of Climate 26 (10)

Dee D, Uppala S, Simmons A, Berrisford P, Poli P, Kobayashi S, Andrae U, Balmaseda M, Balsamo G, Bauer P (2011) The ERA-Interim reanalysis: Configuration and performance of the data assimilation system. Quarterly Journal of the Royal Meteorological Society 137 (656):553-597

Deng L, Wu X (2010) Effects of convective processes on GCM simulations of the Madden-Julian Oscillation. Journal of Climate 23 (2):352-377

Emanuel KA (1987) An air-sea interaction model of intraseasonal oscillations in the tropics. Journal of the Atmospheric Sciences 44 (16):2324-2340

Fairall C, Bradley EF, Godfrey J, Wick G, Edson JB, Young G (1996) Cool-skin and warm-layer effects on sea surface temperature. Journal of Geophysical research 101 (C1):1295-1308

Flatau M, Flatau PJ, Phoebus P, Niiler PP (1997) The feedback between equatorial convection and local radiative and evaporative processes: The implications for intraseasonal oscillations. Journal of the Atmospheric Sciences 54 (19):2373-2386

Gaspar P, Gregoris Y, Lefevre J-M (1990) A simple eddy kinetic energy model for simulations of the oceanic vertical mixing: Tests at station Papa and long-term upper ocean study site. J Geophys Res 95 (C9):16179-16193

Gill AE (1980) Some simple solutions for heat-induced tropical circulation. Quarterly Journal of the Royal Meteorological Society 106 (449):447-462

Hendon HH (2000) Impact of air-sea coupling on the Madden-Julian oscillation in a general circulation model. Journal of the Atmospheric Sciences 57 (24):3939-3952

Hendon HH, Liebmann B (1994) Organization of convection within the Madden-Julian oscillation. Journal of Geophysical Research: Atmospheres (1984–2012) 99 (D4):8073-8083

Hendon HH, Salby ML (1994) The life cycle of the Madden-Julian oscillation. Journal of the Atmospheric Sciences 51 (15):2225-2237

Hsu H-H, Weng C-H, Wu C-H (2004) Contrasting characteristics between the northward and eastward propagation of the intraseasonal oscillation during the boreal summer. Journal of Climate 17 (4):727-743

Hung M-P, Lin J-L, Wang W, Kim D, Shinoda T, Weaver SJ (2013) MJO and convectively coupled equatorial waves simulated by CMIP5 climate models. Journal of Climate 26 (17):6185-6214

Inness PM, Slingo JM (2003) Simulation of the Madden-Julian oscillation in a coupled general circulation model. Part I: Comparison with observations and an atmosphere-only GCM. Journal of Climate 16 (3):345-364

Jiang X, Waliser DE, Xavier PK, Petch J, Klingaman NP, Woolnough SJ, Guan B, Bellon G, Crueger T, DeMott C, Hannay C, Lin H, Hu W, Kim D, Lappen C-L, Lu M-M, Ma H-Y, Miyakawa T, Ridout JA, Schubert SD, Scinocca J, Seo K-H, Shindo E, Song X, Stan C, Tseng W-L, Wang W, Wu T, Wyser K, Wu X, Zhang GJ, Zhu H (2014) Exploring Key Processes of the Madden-Julian Oscillation (MJO): A Joint WGNE MJO Task Force / GEWEX GASS Project on the Vertical Structure and Diabatic Processes of the MJO – Part I. Climate Simulations, submitted.

Kang I-S, Liu F, Ahn M-S, Yang Y-M, Wang B (2013) The Role of SST Structure in Convectively Coupled Kelvin-Rossby Waves and Its Implications for MJO Formation. Journal of Climate 26 (16)

Kim D, Sobel AH, Maloney ED, Frierson DM, Kang I-S (2011) A systematic relationship between intraseasonal variability and mean state bias in AGCM simulations. Journal of Climate 24 (21):5506-5520

Kim D, Sperber K, Stern W, Waliser D, Kang I-S, Maloney E, Wang W, Weickmann K, Benedict J, Khairoutdinov M (2009) Application of MJO simulation diagnostics to climate models. Journal of climate 22 (23):6413-6436

Kiranmayi L, Maloney ED (2011) Intraseasonal moist static energy budget in reanalysis data. Journal of Geophysical research 116 (D21)

Klingaman NP, Woolnough SJ, Weller H, Slingo JM (2011) The impact of finer-resolution air-sea coupling on the intraseasonal oscillation of the Indian monsoon. Journal of Climate 24 (10):2451-2468

Lin J-L, Kiladis GN, Mapes BE, Weickmann KM, Sperber KR, Lin W, Wheeler MC, Schubert SD, Del Genio A, Donner LJ (2006) Tropical intraseasonal variability in 14 IPCC AR4 climate models. Part I: Convective signals. Journal of climate 19 (12)

Lindzen RS, Nigam S (1987) On the role of sea surface temperature gradients in forcing low-level winds and convergence in the tropics. Journal of the Atmospheric Sciences 44 (17):2418-2436

Liu P, Wang B, Sperber KR, Li T, Meehl GA (2005) MJO in the NCAR CAM2 with the Tiedtke Convective Scheme*. Journal of climate 18 (15):3007-3020

Madden RA, Julian PR (1972) Description of global-scale circulation cells in the tropics with a 40-50 day period. J atmos Sci 29 (6):1109-1123

Maloney ED (2009) The moist static energy budget of a composite tropical intraseasonal oscillation in a climate model. Journal of Climate 22 (3):711-729

Maloney ED, Hartmann DL (1998) Frictional moisture convergence in a composite life cycle of the Madden-Julian oscillation. Journal of climate 11 (9):2387-2403

Maloney ED, Sobel AH (2004) Surface fluxes and ocean coupling in the tropical intraseasonal oscillation. Journal of climate 17 (22):4368-4386

Marshall AG, Alves O, Hendon HH (2008) An Enhanced Moisture Convergence-Evaporation Feedback Mechanism for MJO Air-Sea Interaction. Journal of the Atmospheric Sciences 65 (3):970-986

Nakazawa T (1988) Tropical super clusters within intraseasonal variations over the western Pacific. Journal of the Meteorological Society of Japan 66 (6):823-839

Neelin JD, Held IM, Cook KH (1987) Evaporation-wind feedback and low-frequency variability in the tropical atmosphere. Journal of the Atmospheric Sciences 44 (16):2341-2348

Nordeng TE (1994) Extended versions of the convective parametrization scheme at ECMWF and their impact on the mean and transient activity of the model in the tropics. European Centre for Medium-Range Weather Forecasts,

Paulson CA, Simpson JJ (1981) The temperature difference across the cool skin of the ocean. J Geophys Res 86 (C11):11044-11054

Reynolds RW, Smith TM (1995) A high-resolution global sea surface temperature climatology. Journal of Climate 8 (6):1571-1583

Roeckner E (2003) The atmospheric general circulation model ECHAM5: Part 1: model description. Max-Planck-Institut fuer Meteorologie,

Saunders PM (1967) The temperature at the ocean-air interface. Journal of the Atmospheric Sciences 24 (3):269-273

Shinoda T, Hendon HH (1998) Mixed layer modeling of intraseasonal variability in the tropical western Pacific and Indian Oceans. Journal of climate 11 (10):2668-2685

Sperber KR, Gualdi S, Legutke S, Gayler V (2005) The Madden-Julian oscillation in ECHAM4 coupled and uncoupled general circulation models. Climate Dynamics 25 (2-3):117-140

Subramanian AC, Jochum M, Miller AJ, Murtugudde R, Neale RB, Waliser DE (2011) The Madden-Julian Oscillation in CCSM4. Journal of Climate 24 (24):6261-6282. doi:10.1175/JCLI-D-11-00031.1

Tiedtke M (1989) A comprehensive mass flux scheme for cumulus parameterization in large-scale models. Monthly Weather Review 117 (8):1779-1800

Tsuang B-J, Tu C-Y, Tsai J-L, Dracup JA, Arpe K, Meyers T (2009) A more accurate scheme for calculating Earths-skin temperature. Climate Dynamics 32 (2-3):251-272

Tu C-Y, Tsuang B-J (2005) Cool-skin simulation by a one-column ocean model. Geophysical research letters 32 (22)

Waliser DE, Lau K, Kim J-H (1999) The influence of coupled sea surface temperatures on the Madden-Julian oscillation: A model perturbation experiment. Journal of the Atmospheric Sciences 56 (3):333-358

Wang B, Rui H (1990) Dynamics of the Coupled Moist Kelvin-Rossby Wave on an Equatorial-Plane. Journal of the Atmospheric Sciences 47 (4):397-413

Watterson I (2002) The sensitivity of subannual and intraseasonal tropical variability to model ocean mixed layer depth. Journal of Geophysical Research: Atmospheres (1984–2012) 107 (D2):ACL 12-11-ACL 12-15

Watterson I, Syktus J (2007) The influence of air–sea interaction on the Madden–Julian oscillation: The role of the seasonal mean state. Climate Dynamics 28 (7-8):703-722

Wheeler MC, Hendon HH (2004) An all-season real-time multivariate MJO index: Development of an index for monitoring and prediction. Monthly Weather Review 132 (8):1917-1932

Woolnough S, Vitart F, Balmaseda M (2007) The role of the ocean in the Madden–Julian Oscillation: Implications for MJO prediction. Quarterly Journal of the Royal Meteorological Society 133 (622):117-128

Woolnough SJ, Slingo JM, Hoskins BJ (2000) The relationship between convection and sea surface temperature on intraseasonal timescales. Journal of Climate 13 (12):2086-2104

Wu J (1985) On the cool skin of the ocean. Boundary-Layer Meteorology 31 (2):203-207

Yanai M, Chen B, Tung W-w (2000) The Madden-Julian oscillation observed during the TOGA COARE IOP: Global view. Journal of the Atmospheric Sciences 57 (15):2374-2396

Zhang C (2005) Madden-Julian oscillation. Reviews of Geophysics 43 (2)

Zhang C, Dong M, Gualdi S, Hendon HH, Maloney ED, Marshall A, Sperber KR, Wang W (2006) Simulations of the Madden-Julian oscillation in four pairs of coupled and uncoupled global models. Climate Dynamics 27 (6):573-592

Zhang GJ, Mu M (2005) Simulation of the Madden-Julian Oscillation in the NCAR CCM3 using a revised Zhang-McFarlane convection parameterization scheme. Journal of climate 18 (19):4046-4064

Zhou L, B. Neale R, Jochum M, Murtugudde R (2012) Improved Madden-Julian oscillations with improved physics: The impact of modified convection parameterizations. Journal of Climate 25 (4):1116-1136

Zhu H, Hendon H, Jakob C (2009) Convection in a parameterized and superparameterized model and its role in the representation of the MJO. Journal of the Atmospheric Sciences 66 (9):2796-2811

Table Captions

Table 1. List of the experiments. The ECHAM5 AGCM is used in all experiments. The abbreviation of the experiments: "A" means standalone AGCM simulation. "C" means coupled to SIT model. The description indicates key features of the experiments.

Section	Experiments	Ocean model	Description
3.1~3.2	A-CTL	-	Standalone AGCM forced by observed SST climatology
	C-CTL	SIT	Model coupled over the tropical domain (30S-30N), with the finest vertical resolution (1m in the upper 10m)
3.3 a)	C-17m	SIT	The first ocean vertical level starts at16.8 m
	C-59m		The first ocean vertical level starts at 59.3 m
3.3 b)	C-IO	SIT	Coupled in Indian Ocean only. (30˚S-30˚N,50˚E-100˚E)
	C-PO		Coupled in West Pacific only. (30˚S-30˚N,110˚E-180˚E)
	C-IPO		Coupled in Indian Ocean and West Pacific. (30˚S-30˚N,40˚E-180˚E)
3.3 c)	A-OISST	-	AGCM forced by the observed daily SST
	A-day		AGCM forced by the daily SST from C-CTL
	A-clim		AGCM forced by the climatology SST from C-CTL

Figure Captions

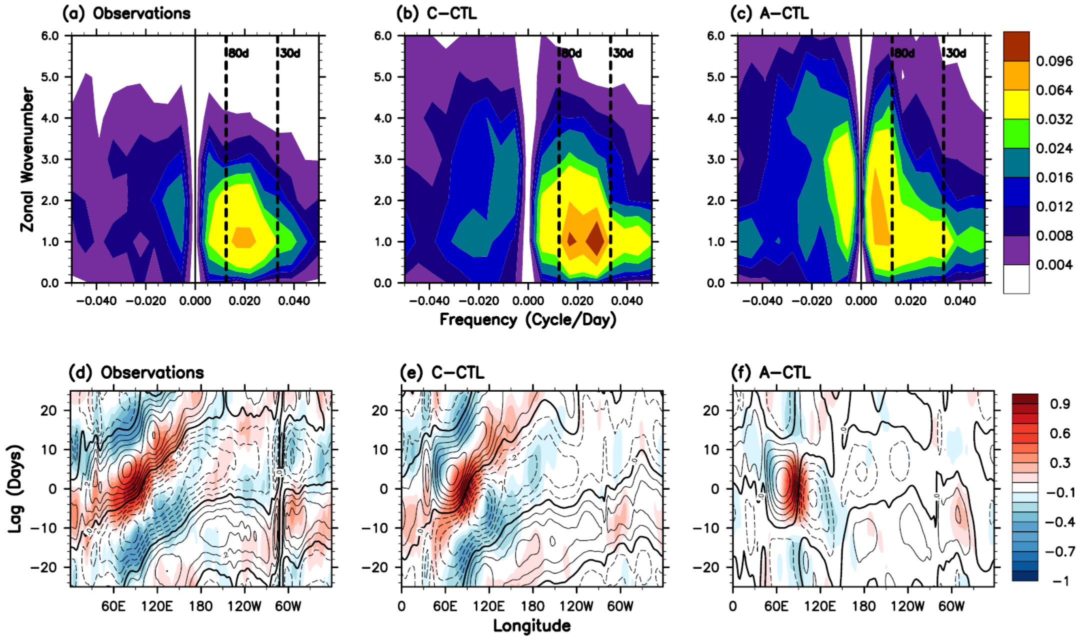

Figure 1. (**a-c**) Zonal wavenumber-frequency spectra for equatorial 850-hPa zonal wind and (**d-f**) Hovmöller diagrams of correlation between the Indian Ocean (10°S-5°N, 75-100°E) precipitation and 10°N-10°S averaged precipitation (color) and zonal wind (contour) on intraseasonal timescale. (**a, d**) are from observations and (**b, e**) and (**c, f**) are from the simulations by the coupled ECHAM5-SIT (C-CTL) and uncoupled ECHAM5 (A-CTL) models (see Table 1), respectively.

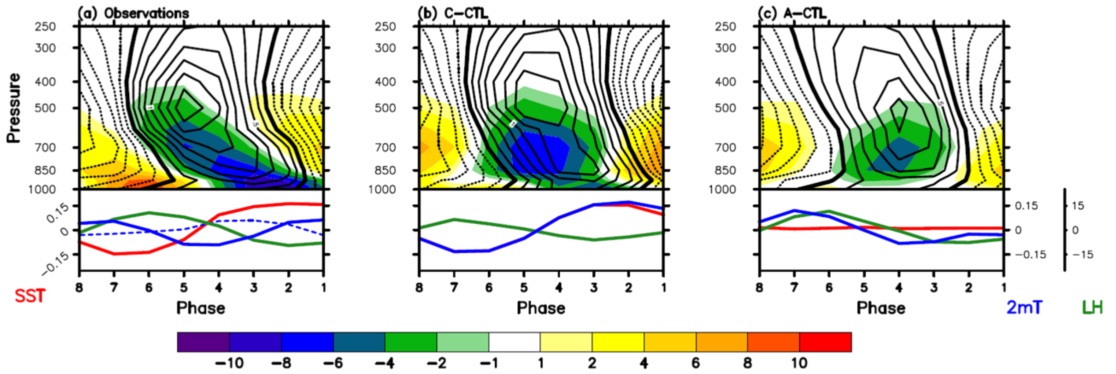

Figure 2. The MJO lifecycle in the Maritime Continent region in **(a)** observations (ERA interim) and simulations by the **(b)** coupled ECHAM5-SIT (C-CTL) and **(c)** uncoupled ECHAM5 (A-CTL) models. Shading shows moisture divergence (10^{-6}·g/kg·1/s) from the surface to the upper troposphere; negative values indicate convergence. Overlaid contours show the equivalent potential temperature(θ_e; K). Contour interval is 0.025; solid (dashed) lines are positive (negative) values. (Lower panels) SST (°C, red), latent heat flux (W/m^2, green; positive is upward) and 2 meter air temperature (℃, blue) anomalies. The 2m-air temperature from NCEP Reanalysis II is shown in (a) for comparison (blue dashed). Phase 1 is the earliest of the eight MJO phases, and phase 4 is the active phase when convection is strongest over the Maritime continent. The phase from 8 down to 1 implies the zonal direction. All parameters are averaged over the region 10°S-0°N, 120-150°E.

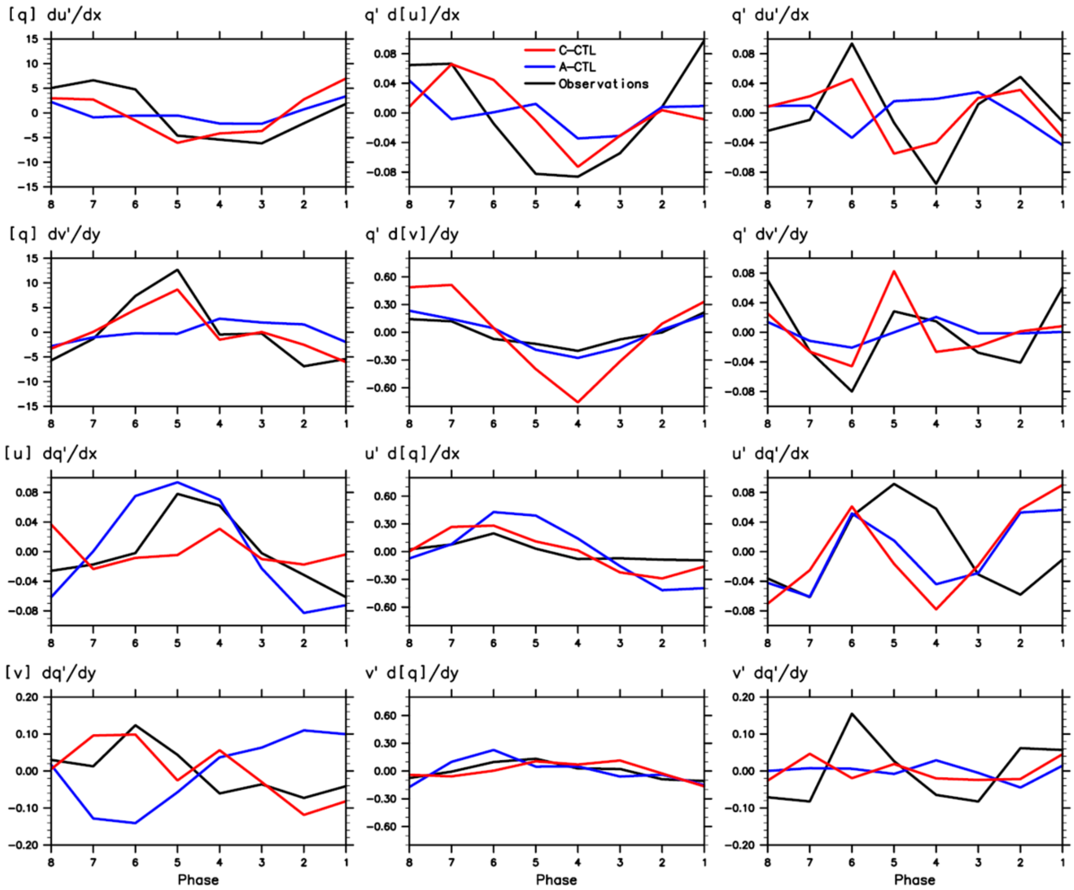

Figure 3. Anomalous moisture divergence components ($10^{-6}\cdot$g/kg$\cdot$1/s) at 1000hPa averaged over the maritime region (10°S-0°N, 120-150°E) during the eight phases of the MJO for observations (black), and simulated by the (red) coupled ECHAM5-SIT (C-CTL) and (blue) uncoupled ECHAM5 (A-CTL) models. The observed terms are computed from the ERA-Interim reanalysis (Dee et al. 2011). q is specific humidity, and $\vec{u}$ is vector wind. Brackets are climatological means, and primes are intraseasonal anomalies. Note the different vertical scales between panels.

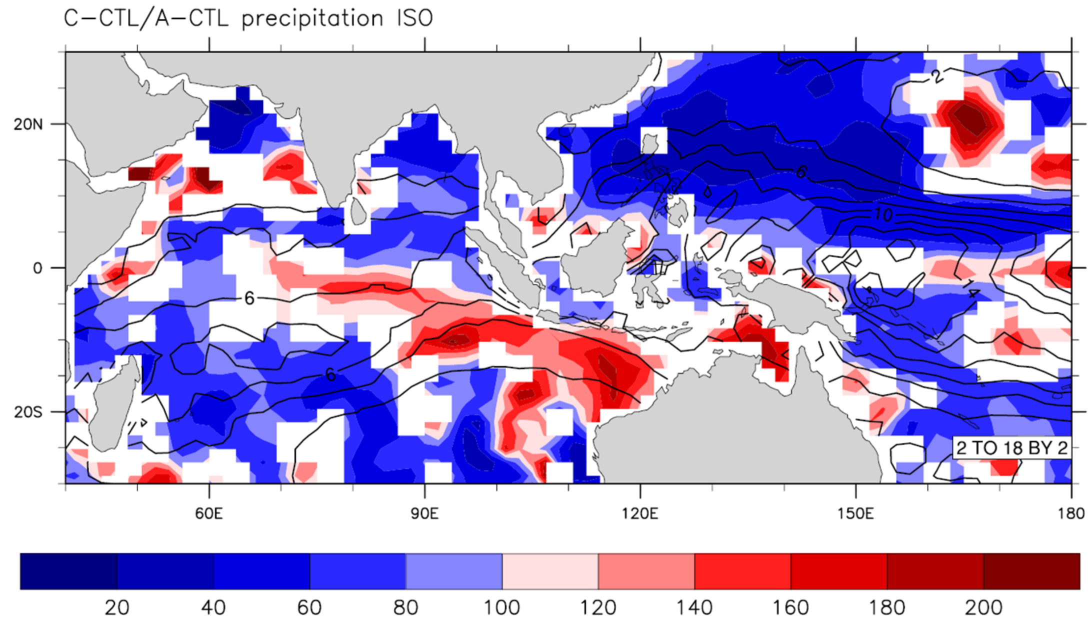

Figure 4. The ratio of the precipitation variance between the coupled ECHAM5-SIT (C-CTL) and uncoupled ECHAM5 (A-CTL) models on intraseasonal time scales. The colour areas mark where the ratio is statistically significant at 1% based on an F-test. The contours show the mean precipitation of the A-CTL.

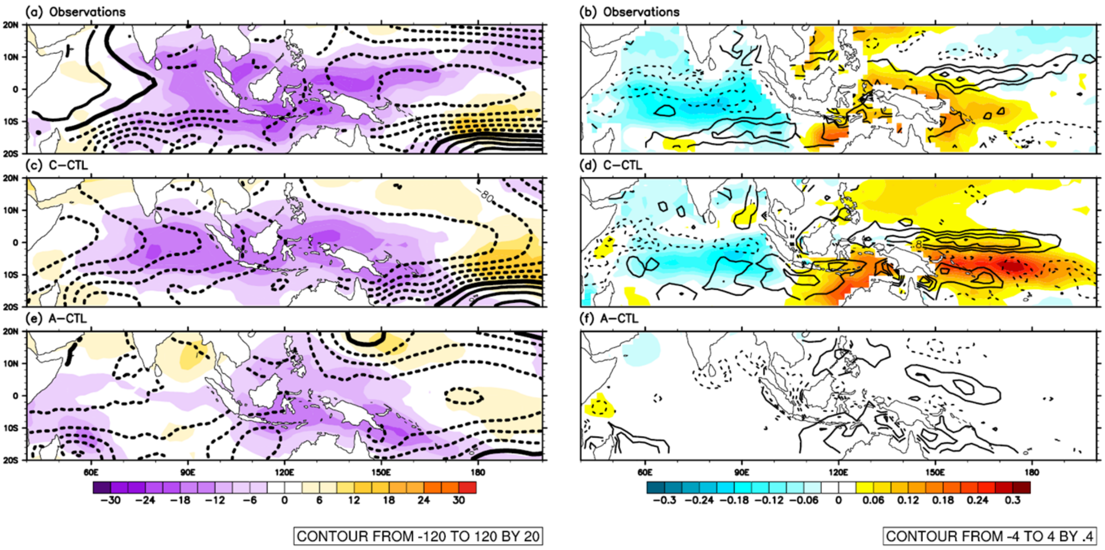

Figure 5. Composites for MJO phase 4 when deep convection is the strongest over the Maritime Continent: (**a, c, e**) OLR (W/m^2, shaded), SLP (Pa, contours) and (**b, d, f**) SST (K, shaded), 10 meter horizontal convergence (10^{-6} 1/s, contours, solid line indicating convergence). (**a, b**) are from observations and **(c, d)** and (**e, f**) are from simulations by the coupled ECHAM5-SIT (C-CTL) and uncoupled ECHAM5 (A-CTL) models, respectively.

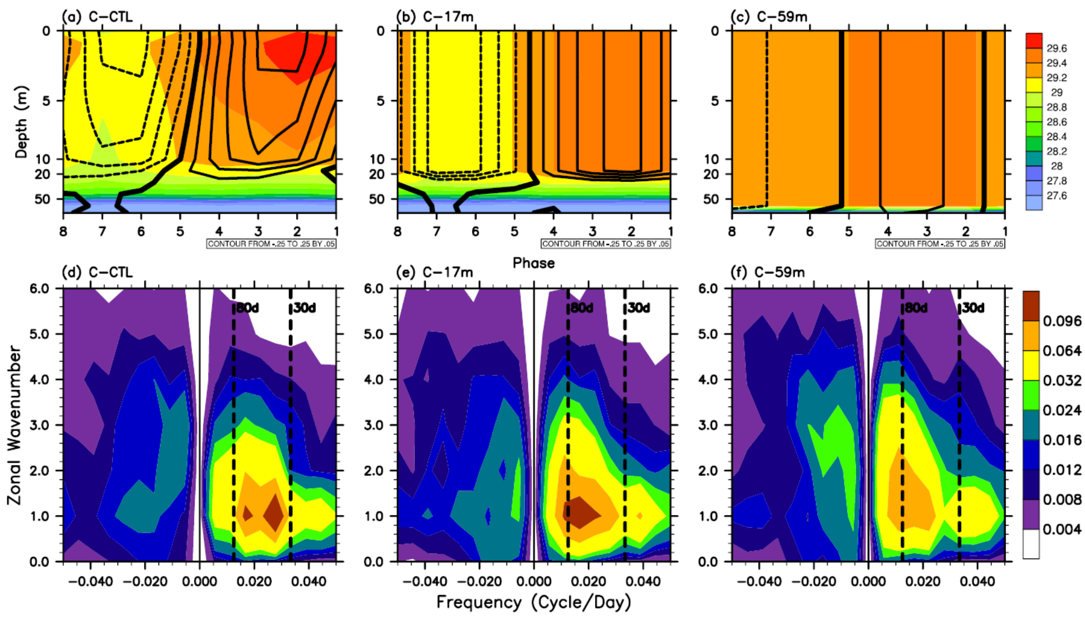

Figure 6. Upper ocean potential temperature (°C) variations at 2.5°S, 130°E over the eight MJO phases simulated with ECHAM5-SIT coupled model with vertical resolutions of (**a**) 1m in the ocean upper 10m (C-CTL), and with top ocean grid cells of (**b**) 16.8m (C-17m) and (**c**) 59.3m (C-59m). Temperature is shaded and anomaly is contoured with an interval of 0.05℃. Note the non-linear depth axis. (**d, e, f**) Corresponding zonal wavenumber-frequency spectra for the equatorial 850-hPa zonal wind.

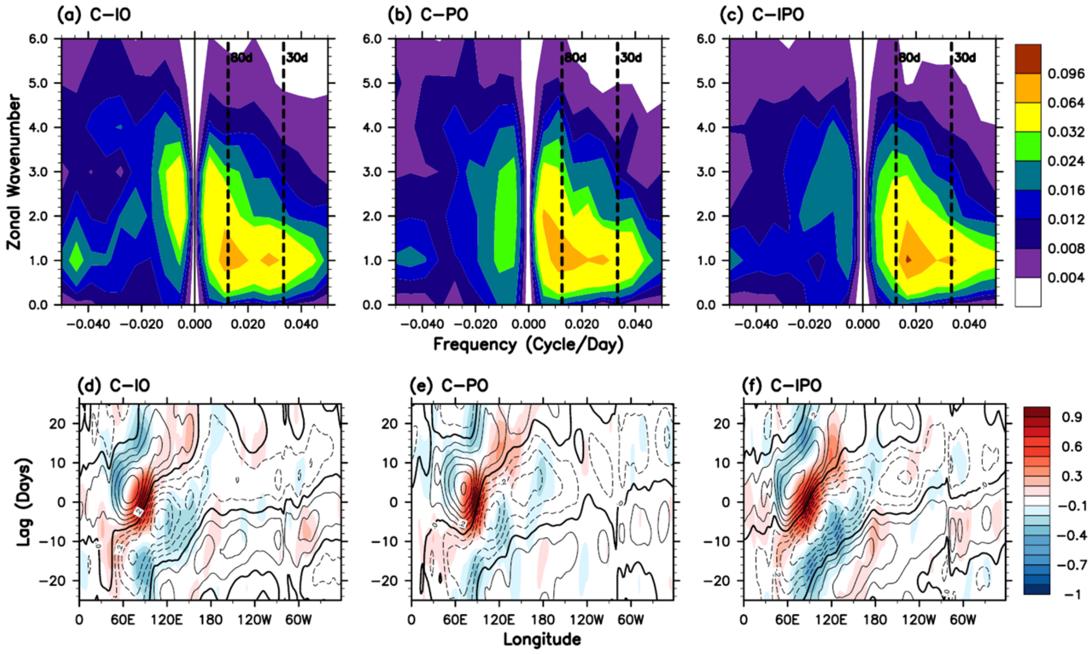

Figure 7. Same as Fig. 1 except for **(a, d)** C-IO, coupling region 30°N-30°S, 50°E-100°E; **(b, e)** C-PO, coupling region 30°N-30°S, 110°E-180°E; and **(c, f)** C-IPO, coupling region 30°N-30°S, 40°E-180°E.

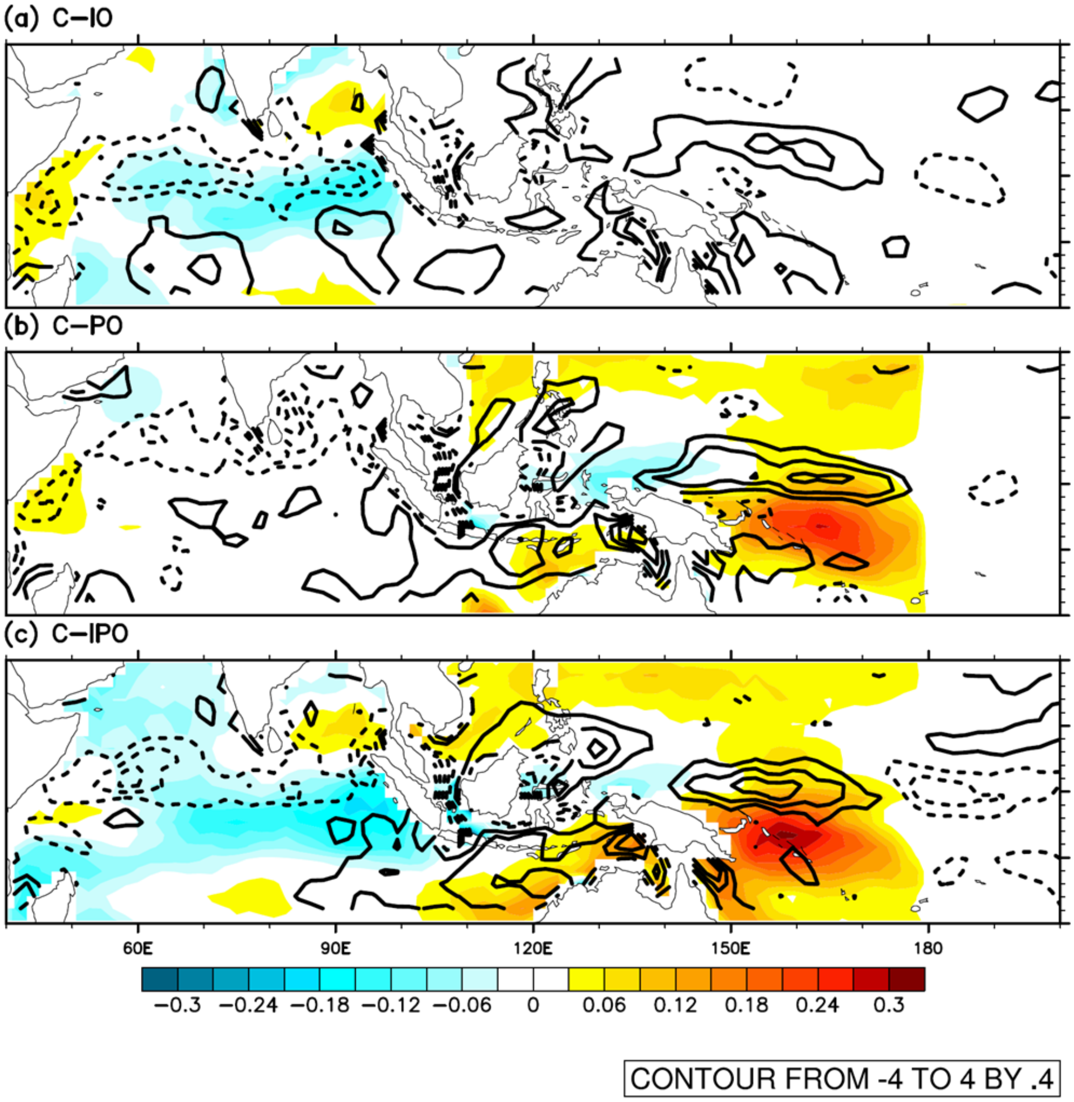

Figure 8. Composites for MJO phase 4 when deep convection is the strongest over the Maritime Continent: SST (K, shaded), 10 meter horizontal convergence (10^{-6} 1/s, contours, solid line indicating convergence) from **(a)** C-IO **(b)** C-PO and **(c)** C-IPO.

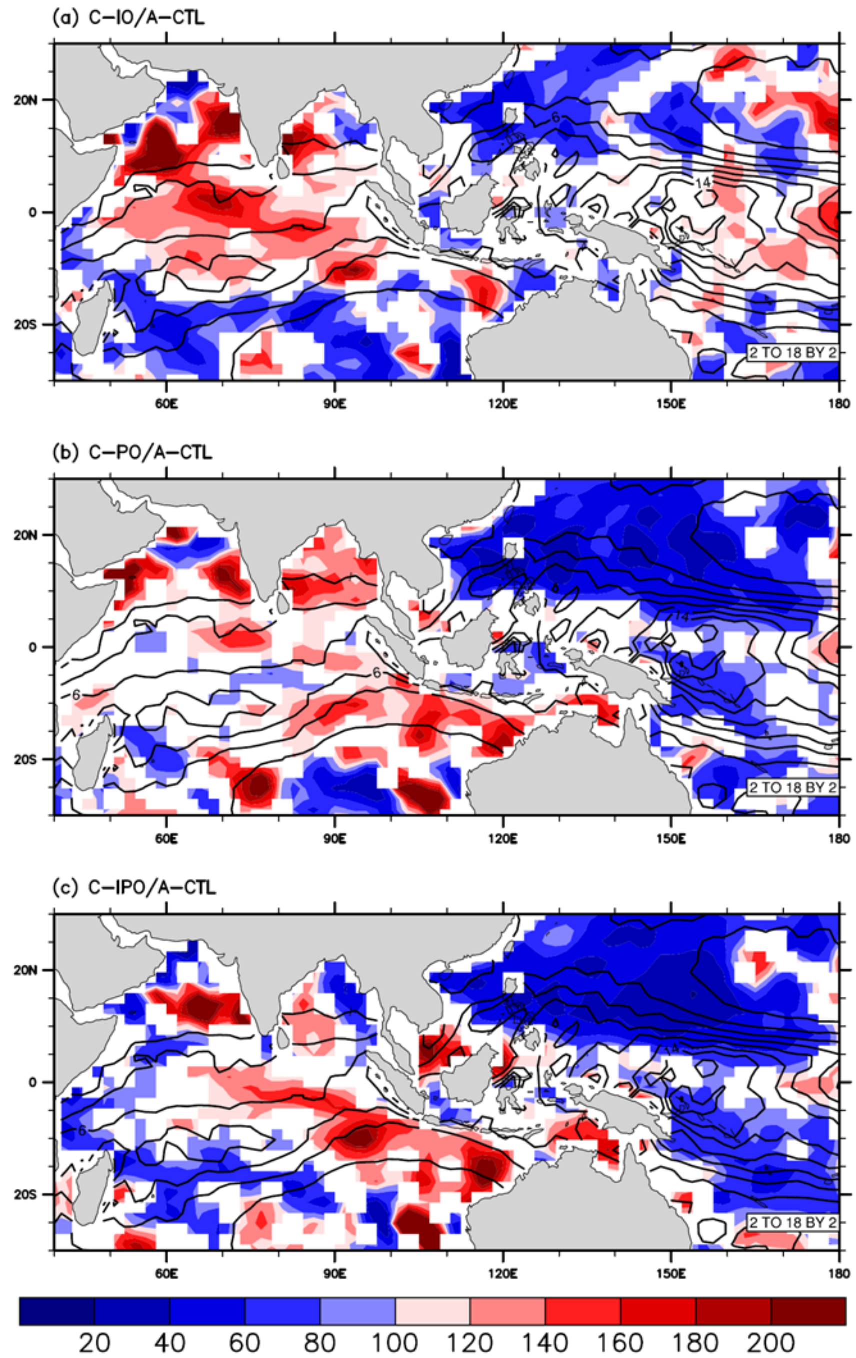

Figure 9. Same as Figure 4 except for **(a)** C-IO, **(b)** C-PO and **(c)** C-IPO.

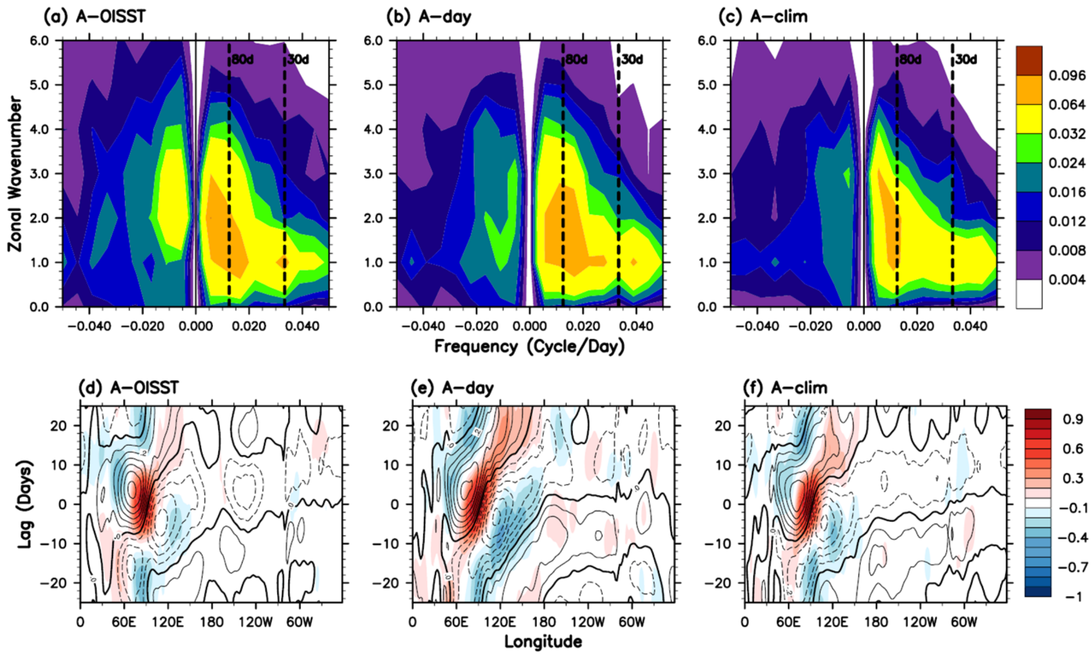

775

776 **Figure 10.** Same as Fig. 1 except for **(a, c)** A-OISST, **(b, d)** A-day and **(c, f)** A-clim

777 simualtions.

778

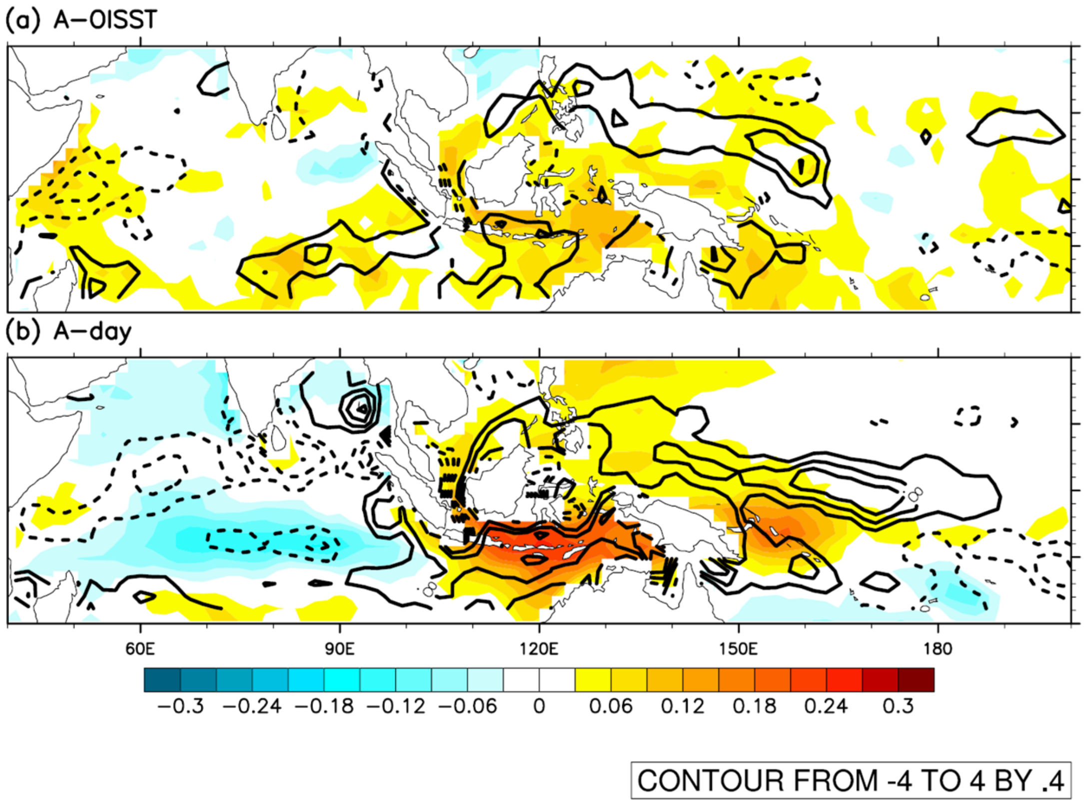

Figure 11. Same as Fig. 8 except for **(a)** A-OISST and **(b)** A-day.

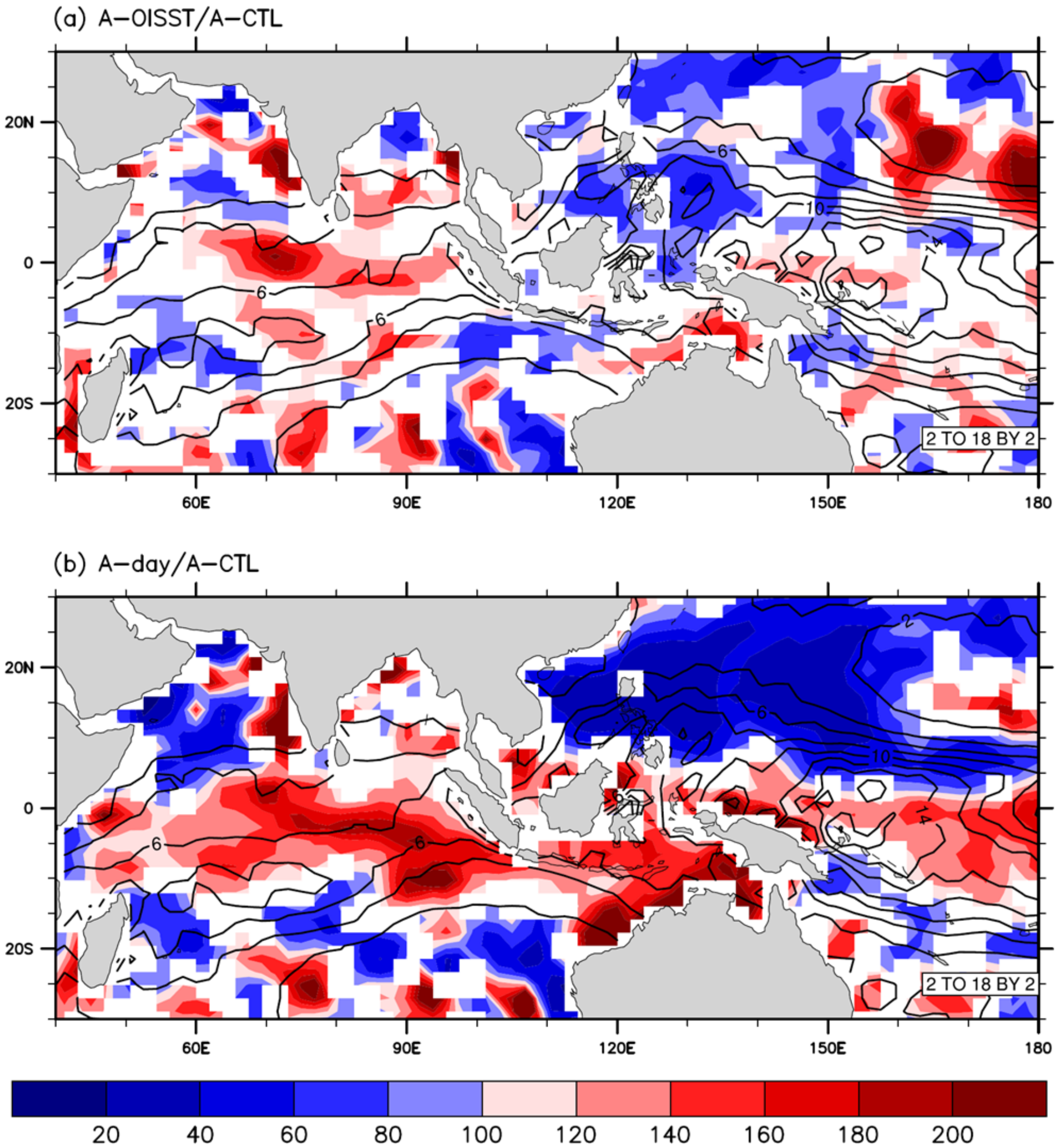

Figure 12. Same as Figure 4 except for **(a)** A-OISST and **(b)** A-day.

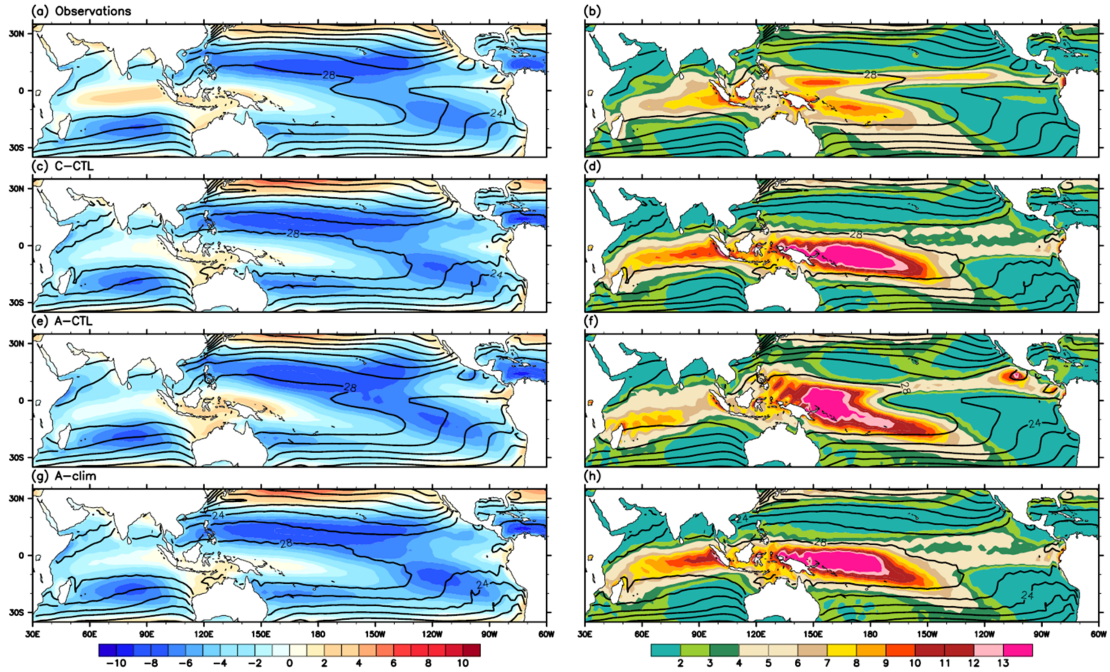

Figure 13. The mean winter (DJF) conditions from **(a, b)** observations and simulations by **(c, d)** C-CTL, **(e, f)** A-CTL and **(g, h)** A-clim. Shading shows (left) 10 m zonal wind (m/s) and (right) precipitation (mm/day), with SST contour overlaid (°C, contour). Observed precipitation are from GPCP (Adler et al. 2003), 10 m zonal wind from ERA Interim reanalysis, and SST from NOAA.

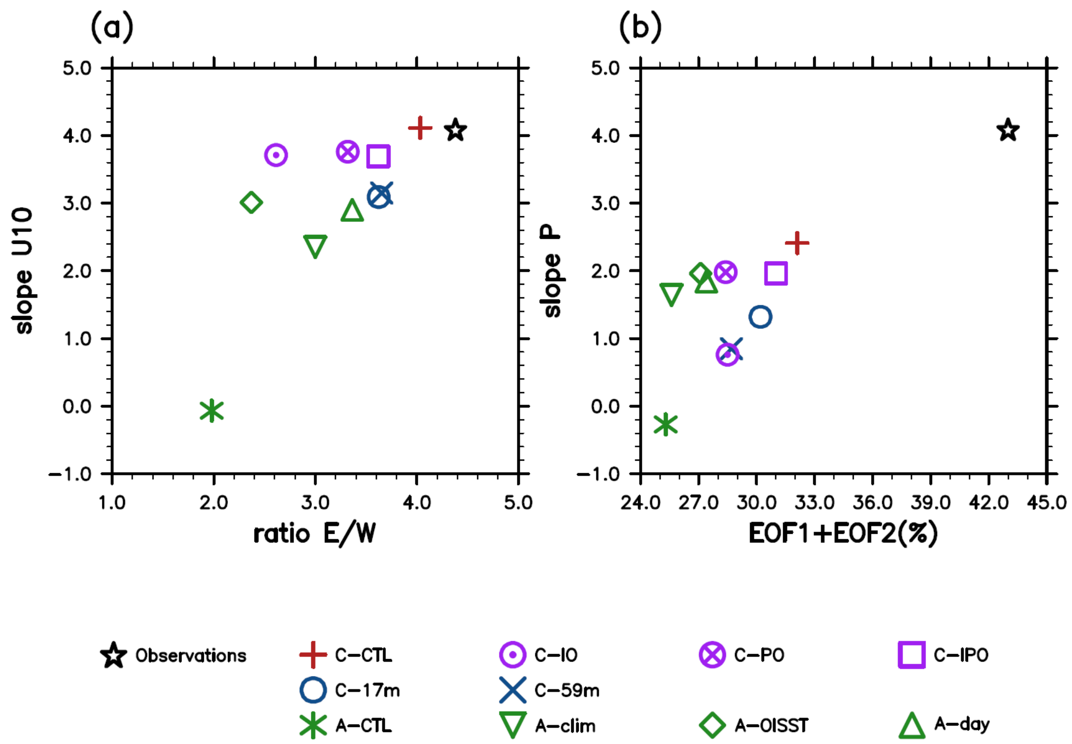

Figure 14. Scatter plots of various MJO indices in observation and ten experiments (Table 1). **(a)** X-axis is the power ratio of east/west propagating waves. The east/west ratio is calculated by dividing the sum of eastward propagating power by the westward propagating counterpart within wavenumbers 1–3 (1–2 for zonal wind), period 30–80 days. Y-axis is the eastward propagation speed of 10 meter zonal wind anomaly. **(b)** X-axis is the sum of the RMM1 and RMM2 variance based on (Wheeler and Hendon 2004). Y-axis is the eastward propagation speed of precipitation anomaly. Numbers marked in the plots were inferred from plots similar to Fig. 1.

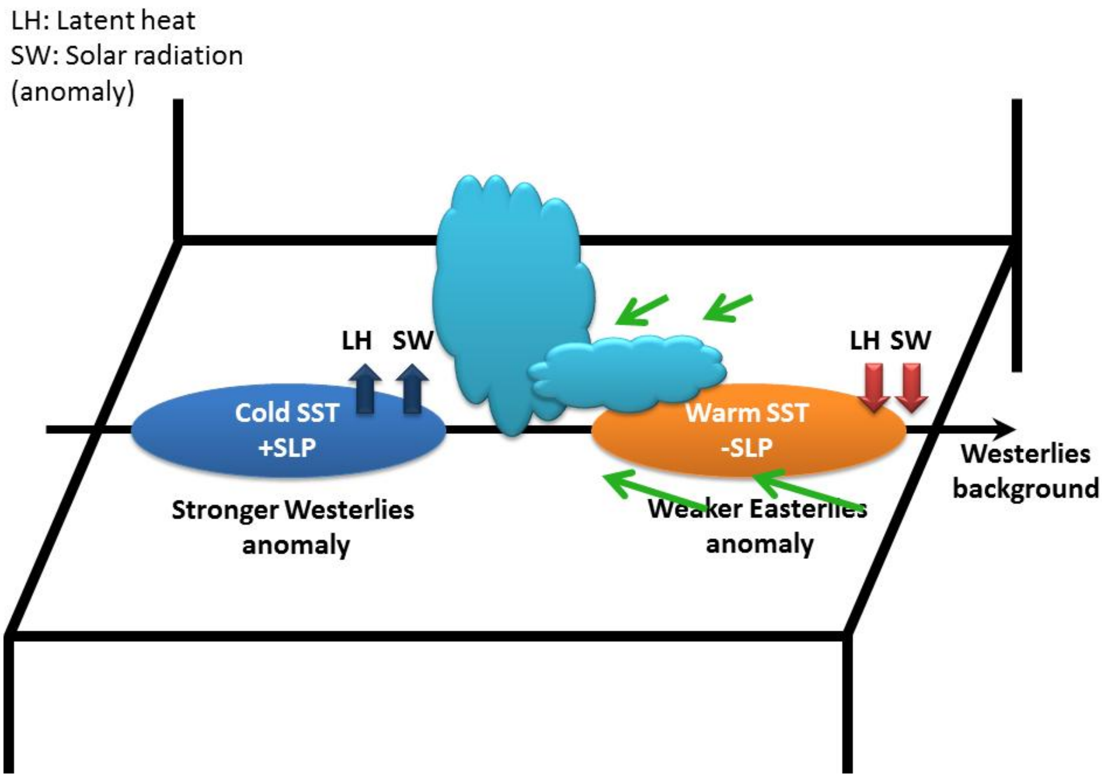

Figure 15. Schematic of the MJO mechanism identified from observations and coupled ECHAM5-SIT simulations. A combination of Frictional Wave-CISK mechanism (Wang and Rui 1990) and ASCII (Flatau et al. 1997) is proposed: To the east of organized deep convection there is increased incident short wave radiation due to clear sky conditions, and reduced latent heat flux (evaporation) from weaker wind speed. These drive warming of the upper ocean that in turns causes anomalously low SLP by inducing Kelvin-wave like perturbation and enhances the low-level atmospheric convergence. The latter leads to enhanced low-level moisture and preconditions deep convection and eastward propagation of deep convection. To the left, stronger winds enhance evaporation and latent heat flux loss, cooling the ocean; while under the deep convection short wave radiation is reduced and also cools the ocean. Weaker winds

ahead of the deep convection and stronger winds following drive shallow and deep upper ocean mixed layers, respectively.